2011 IEEE/RSJ International Conference on
Intelligent Robots and Systems
September 25-30, 2011. San Francisco, CA, USA

FAS A flexible Antagonistic spring element for a high performance over actuated hand

Werner Friedl, Maxime Chalon, Jens Reinecke and Markus Grebenstein
Institute of Robotics and Mechatronics, German Aerospace Center (DLR), Wessling, Germany
E-mails: {Werner.Friedl, Maxime.Chalon, Reinecke.Jens, Markus.Grebenstein }@dlr.de

***Abstract*— In robotic hands design tendon driven systems have been considered for years. The main advantage is a small end effector inertia e.g. a light, small hand with high dynamics due to remote actuators. To protect the actuators from impact in unknown environments a compliant mechanism can be used. It absorbs energy during an impact or saves energy to enhance the joint dynamics. In this paper an antagonistic tendon mechanism is presented. It fits 38 times in the DLR Hand Arm System forearm and enables is adapted to the different finger joints and different tendon lengths. A magnetic sensor was developed for the force measurement of the tendons. Finally, the calibration and the robustness are demonstrated through a set of experiments.**

I. INTRODUCTION

The development of highly dynamic robots which are also robust against impacts is one of the main motivation for the design of the anthropomorphic hand arm system [1] at DLR (Fig. 1). At such system scale, the robustness is commonly achieved by the means of flexible joints or links. The pros and cons of flexible joint mechanisms have been presented in numerous papers [2]–[4].

To provide joint flexibility on a hand with 19 degrees of freedom, McKibben actuators like in the Shadow hand [5] can be used. However,electro motors are selected due to their mobility and efficiency. Indeed, the efficiency of pressurized air generation is only 25 percent. The approach of the ACT hand is to use a motor in parallel to a synthetic passive tension composite material tube. It fits well to the human hand model, but was not developed to fit 38 times into a forearm. There exist two main approaches to provide variable stiffness tendon driven systems. The first one is to use the tendon to actuate a spring mechanism [6]–[9], the second one is to integrate the mechanism into the output of the actuator. [10]–[14]. The second group can be differentiated in systems which preload a nonlinear spring or systems which change the length of a lever arm to change the stiffness. The advantage of e.g. the Floating Spring Joint [15] as arm joint which uses a small motor for the stiffness variation and a big motor for the joint motion, cannot be implemented in the forearm because the tendon travel for flexors and extensors is not symetric w.r.t the wrist and finger configurations. If rigid tendons were to connect directly the gear output and joint without an additionally elastic element, the tendon would break [16]. Floating spring, such as in [8], are difficult to integrate because the mechanism position is not defined when the tendon has no load. Moreover, it results in an increased tendon inertia. The points shown above and the creep of the tendons (Fig. 3) lead to the choice of an antagonistic configuration. Based on the mechanism shown in [6], a new mechanism that fits 38 times into the forearm has been designed. It can be tuned to the different needed force to deflection behaviors by modifying the equilibrium point, the spring rate and the spring position regarding the lever.

In this paper the development of a highly integrated variable stiffness element is presented. In the first section, the mechanism is presented along with the constraints it has to fulfill. A second section presents the test system used to verify and calibrate the sensors. Finally, the third section gives primilinary results on the tendon force control performance, that can be achieved using this sensor.

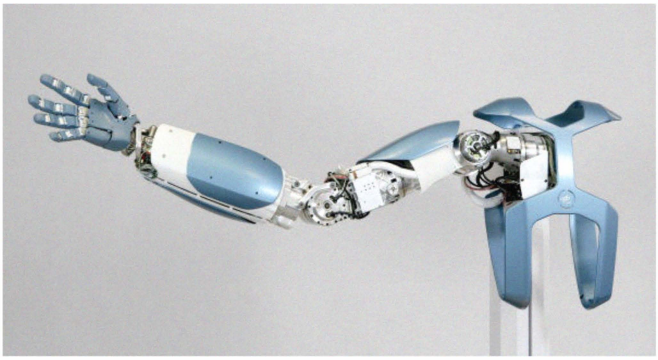

Fig. 1. DLR Hand Arm Sytem

II. THE LEVER MECHANICS

A. Requirements

One of the focuses of hand-arm systems is how to match the human archetype regarding performance, size and weight. To achieve human like fingertip forces and stiffness behavior several spring characteristics are needed, since the tendons have different levers in the fingers. The thumb, index, middle and little finger have four degrees of freedom (DOF), the ring finger has only three, because PIP (proximal inter phalangeal) and DIP (distal inter phalangeal) joint are coupled. Since the actuation is using a $2n$ tendons scheme, a total of 38 tendons are required to control the position and the stiffness of all the joints. Unlike humans, the extensors are as strong as the flexor actuators in order to standardize the actuation units.

978-1-61284-456-5/11/$26.00 ©2011 IEEE

The required tendon forces are ranging from 60N for the metacarpal joint of the little finger and rising up to 350N for the DIP joint of the index finger. All joints should have a passive range of 30 degrees without tendon slack. Hence one mechanism must provide 60 degree tendon travel at the finger. Despite all these requirements the mechanism must remain compact, with low friction and minimal inertia.

B. Tendon material selection

The quality of a progressive stiffness element depends strongly on the type of the tendon used. Several commercial ropes or cables are available. They must provide a combination of qualities. In case of the hand-arm system the following characteristics are needed:

- The tendon must be durable.
- The material must have a minimal bending radius to minimize the diameter of pulley.
- It must be feasible to attach the tendon with slices or nodes.
- The tendon must withstand about 350N.
- The tendon must provide a minimal friction with the sliding surfaces.

Therefore, a test bed was built with the ability to run the tendons on diverse pulley diameters in order to compare different tendon materials. A durability test in rolling conditions was performed using two pulleys with variable diameter redirecting the tendon coming from a motor to a spring. For sliding tests a glide surface similarly to the finger can be mounted [16]. All tests were performed until tendon failure (detected by a comparison between the spring force and the motor torque). The tests using steel tendons showed very low durability. The dyneema ropes revealed 200 times better lifetime and double maximum force. Moreover, the dyneema rope can be spliced. This results in a compact and reliable ending. On the contrary, the steel tendons are difficult to terminate on site and a pinching of the tendon during assembly would severely damage the cable [16]. However, due to its structure, the dynema rope elongation is one-third higher than for the steel cable due to the lower Young's modulus. Moreover, the dyneema tendons have creep (Fig.3). Therefore a pretension controller is required to maintain the tendon forces. The relatively long tendon lengths (up to 400 mm) are creating a serial stiffness that must be included in the mechanism design.

C. Design

Based on the elementary angle correlation in a triangle (Fig. 4) the mathematical model of a version without any pulleys is illustrated. The deflection of the mechanism is calculated by the function:

$$s = s_0 - \frac{-2L}{\cos\alpha} \tag{1}$$

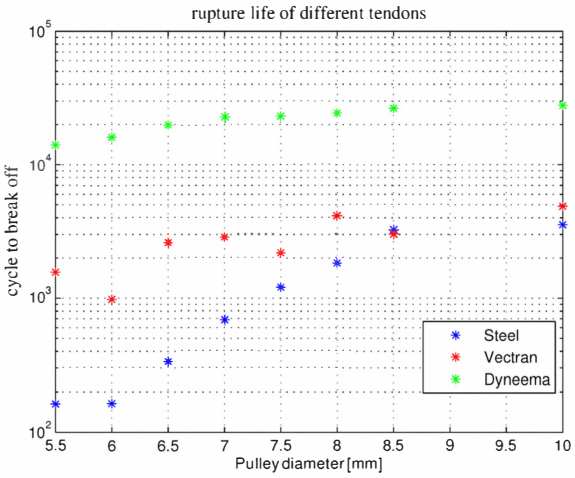

Fig. 2. Comparison of different tendon materials

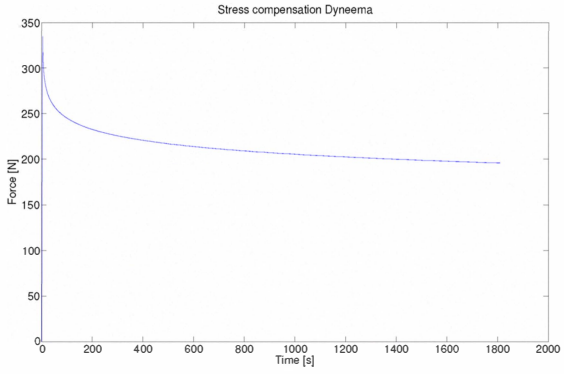

Fig. 3. Strain relaxation curve of a dyneema tendon under imposed constant displacement

The parameter s_0 depends on the start angle alpha zero. If the equitation is solved for α, it yields.

$$\alpha := \arccos(\frac{-2L}{s_0 - s}) \tag{2}$$

The next step is the force curve depending on alpha:

$$F = \frac{0.5\ F_s}{\sin(\alpha)} = \frac{0.5\ c\ (sw_0 - L\ \sin(\alpha))}{\sin\ \alpha} \tag{3}$$

The start length sw_0 of the spring depends again on α and c is the spring rate. Replacing α with the formula (3) gives:

$$F(s) = -0.5\ \frac{c(-sw_0 + L\ \sin(\pi - \arccos(\frac{2\ L}{s_0 - s})))}{\sin(\pi - \arccos(\frac{2\ L}{s_0 - s}))} \tag{4}$$

The testbed mechanism shown in [6] was easy to build , but for the forearm it must be improved for a space saving variant. Through the hyper actuation of the robotic hand compared to the human the first design goal was to find a solution for the integration of all 38 motors for the hand into the forearm. A human forearm has only 19 muscles for the wrist and finger actuation. Fig. 5 shows three concepts based on exchangeable motor modules.

Concept a) was selected because the motor modules are easily accessible and because it allows a simplified design

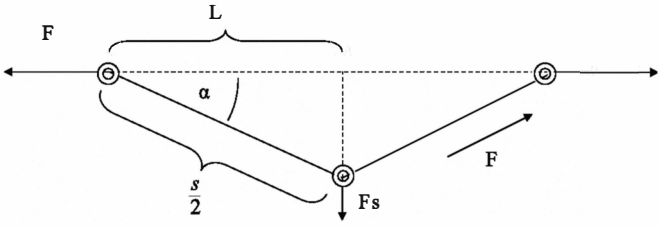

Fig. 4. Sketch of simplified mechanism

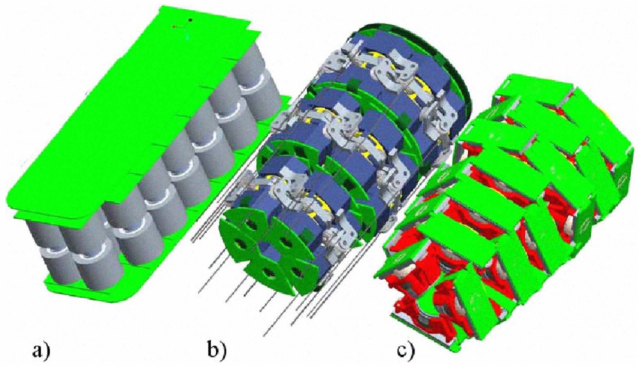

Fig. 5. Initial concept for the forearm: a) Good accessibility for modules and tendons. In b) and c) show more human proportion but complicated tendon routing

for all electronics. The upper half can be opened in order to access the tendons.

D. Dimensioning

To obtain the required stiffness characteristics, the inital position of the spring, the spring rate and the y position(see Fig. 6 of the lever can be selected. The rest of the parameters are imposed because the tendon routing and motor positions are given. The following equations apply only to the Flexible Antagonistic Spring elements (FAS) in the sides of the forearm (see Fig.16). The ten FAS in the middle are similar except the fact that the spring pivot point of the lever can rotate around the lever axis. This was required to simplify integration. All used parameters are reported in the sketch

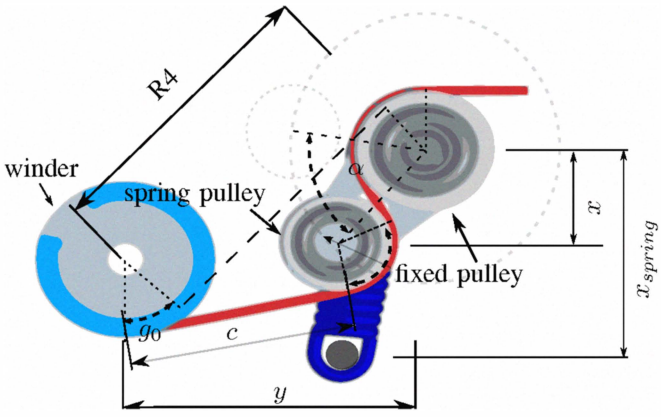

Fig. 6. Sketch of the FAS

(Fig.6) and Table I.

TABLE I
PARAMETERS OF STIFFNESS CURVE EQUATION

Name	Description
α	Angle between lever and lever position at infinite force
β	Angle about the fixed pulley is rotated
$\gamma 0$	start angle of contact on the winder
δ	angle between R0 and R4
R4	straight distance between Winder an fixed pulley
R2	distance between spring pulley and fixed pulley
Rw	Radius of the winder
Rsr	Radius of spring pulley
Rfr	Radius of fixed pulley
rh	length of the lever arm for the spring
rf2	length of the unloaded spring

The deflection of the mechanism calculates to:

$$s = (c + d + (\alpha + \gamma_0)\ Rfr + \gamma_1 Rw + Rsr(\gamma_0 + \alpha - \gamma 1)) - s_0 \tag{5}$$

The distance d follows:

$$d = \sqrt{R4^2 - (Rw + Rfr)^2} \tag{6}$$

The tendon length c is dependent of e :

$$c = \sqrt{e^2 - (Rw + Rsr)^2} \tag{7}$$

e is the direct distance between spring pulley and winder

$$e = \sqrt{R2^2 + R4^2 - 2\ R2\ R4\ \cos(\alpha_0 - \alpha + \beta)} \tag{8}$$

Using the maximum angle $alpha_0$ of the lever the intersection between the displaced line R0 of the spring pulley and the lever working radius rh is needed. The solved formula has two solutions, in which the bigger one p is used. The smaller solution is on the wrong side of the lever.

$$\alpha_0 = \arccos(\frac{p}{R2}) \tag{9}$$

All other angles calculate as follows:

$$\beta = \arcsin(\frac{x}{R4}) \tag{10}$$

$$\delta = \arccos(\frac{R0}{R4}) \tag{11}$$

$$\gamma_0 = \delta + \beta \tag{12}$$

$$\gamma_1 = 0.5\pi + \arctan(\frac{-x + R2\ \sin(\alpha - \alpha 0)}{-y + R2\ \cos(\alpha - \alpha_0)}) + \arccos(\frac{-Rw + Rsr}{e}) \tag{13}$$

The modulus of elasticity and the complete length of the tendon flows in the computation of the start angle. The tendon elongation Δl at maximum force is:

$$\Delta l = \frac{\sigma}{E}\ l = \frac{Fmax}{A\ E}\ l \tag{14}$$

The deflection of the mechanism is the difference of required s and the tendon elongation Δl .

$$s_{lever} = 2\ s_{max} - \Delta l = 2\ \frac{30\deg\ r_{joint} 2\ \pi}{360} - \Delta l \tag{15}$$

After insertion of (15) in (5), $alpha_{start}$ can be solved. The x coordinate of the spring can be given by the intersection of lever radius rh and the rest length of the spring. Due to the springs, which are located in the half distance of the motors to safe volume (see Fig. 16), the y coordinate is fixed. The spring deflection is calculated by the intersection point of spring radius and lever radius R2.

$$fw = fw1 - rf2$$
$$fw1 = \sqrt{(rv - (rh\cos(\alpha - \alpha_0))^2 + (m_0\ rh\sin(\alpha - \alpha_0^2))} \quad (16)$$

m_0 is the distance between lever rotating point and spring fix and calculates to:

$$m_0 = \sqrt{rf2^2 - (rv - rh\cos(\alpha_{start} - \alpha_0)^2} + rh\sin(\alpha_{start} - \alpha_0) \quad (17)$$

With the spring deflection the resulting tendon force can be calculated.

$$F = \frac{F_s}{2\sin(\frac{\gamma_0 - \gamma_1 + \alpha}{2})} \quad (18)$$

F_s is the force on the spring pulley:

$$F_s = \frac{M_h}{R2\sin(\omega + 0.5(\gamma_0 + \gamma_1 + \alpha))} \quad (19)$$

to the tendon at infinite force.

$$\omega = \arcsin(\frac{d}{R2}) \quad (20)$$

The lever torque Mh is the spring force transmitted to the lever.

$$M_h = (F0 + fw\ c) + \cos(\epsilon - \frac{\pi}{2})rh \quad (21)$$

To get the normal force on the lever the angle ϵ is needed.

$$\epsilon = \arccos(\frac{(\sqrt{rv^2 + m_0^2})^2 - rh^2 - fw1}{-2rh\ fw1} \quad (22)$$

Due to the complexity of F and s, no symbolic solution can be found. A vector based on interpolation points is used to get a fit function of the force curve depending on the deflection.

$$f(s) = \sum_{\alpha_{start}}^{\alpha_{max}} [F(\alpha)s(\alpha)] \quad (23)$$

The joint torque is obtained by the superposition of the two curves. The inital pretension value is half of the maximum deflection to avoid tendon slack.

$$\tau = \tau_1 - \tau_2 = f_1(s + s_{lever})r_{joint} - f_2(s + s_{lever})r_{joint} \quad (24)$$

The curves in figure 7 show the behavior of the metacarpal joint of the index finger. The stiffness curve shows at high tendon loads a degressive behavior because of the low tendon stiffness.

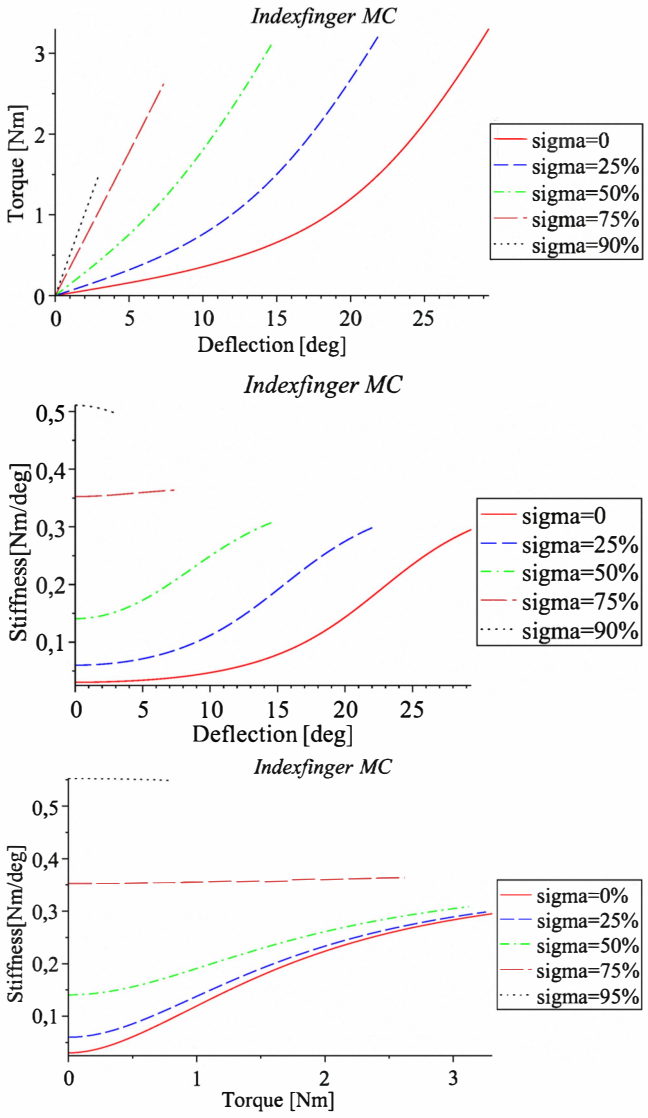

Fig. 7. System behavior of the index finger metacarpal joint (parameters: smax =4.2; Fmax=160; rv=5.5; l=203; x=8.2; y=19.5; R2 =9; R4=21.15; Rw=5.5; Rsr=3.75; Rfr=4.5

E. Sensor

For the control of the hand, a force sensor is necessary. Although no link side sensors are implemented, the measurement of the lever angle α provides all the needed information. Potentiometers were discarded, due to the exposed slider and the high costs of a specially designed PCB. Instead a magnet shape was developed to use a purchasable axial sensor as an off-axis sensor. The MH sensor from ICHAUS is the same as used in the motor modules [1]. It provides a resolution of 12 bits, a small power consumption and minimal volume. The communication interface BISS allows to connect eight sensors in one chain, which saves connections. The main requirement is the measuring range of 45 degrees. A simplified sensor model was used to calculate the two optimal sensor traces. The outer trace consists of positive sin and co sinus hall elements(HEs,HEc), the inner trace consists of negative hall element (HEnc, HEns). The

combined signals of the two hall sensors of each trace provide the angle $omega$.

$$\omega = arctan(\frac{HEs - HEns}{Hec - HEnc}) \\ = arctan(\frac{HEs - HEnc + phase}{(HEs + phase) - HEnc}) \quad (25)$$

The length of a magnetic pole depends on the distance to the rotation centre Dr and the measuring range mr.

$$magnetlength = Dr\ mr \quad (26)$$

For each Dr an optimum mr exists, because the distance between the hall elements is fixed. A phase shift occurres on the cos and the nsin hall element if the required mr different to the optimum. The MH sensor was intended originally designed as an axial sensor hence the arrangement of the hall elements appear at the first sight to be a handicap for an off-axis use. The hall element sequence is sinus, cosinus, negative sinus and at least negative cosinus. For an ideal off-axis sensor the sequence for the negative hall elements should be switched. Because otherwise the negative elements erase partly the positive ones in the sensor model. If the magnets are designed for one trace, the resulting magnetic field on the second trace can compensate the nonlinear sensor behavior. The factor between the two traces has been found by a least square optimization. The real magnet shape has been simulated in Ansys. Two different shapes were found. The optimal one (Fig. 8 above) is very expensive to manufacture. Instead cog magnets were made, which are cheaper but have a reduced linearity. The sensor with this magnet shape is very prone to deviation of the radial distance between magnet and sensor. The nonlinearity of the measured sensor is maximum

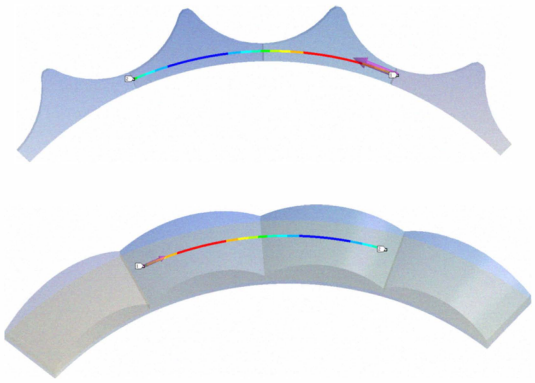

Fig. 8. Two simulated magnet shapes. Top magnet is used in the forearm. The colored line shows the simulated magnet field of one of the traces

3.5 percent. This is due to errors in the manufacturing of the magnet.

III. Test Setup

Before the final assembly of the forearm all lever sensors are calibrated to obtain the stiffness curves. A force gauge is mounted on the tendons to measure the forces. All angle sensor data's are collected by the space wire driver. For the force sensor an AD card from NI is used. A QNX system is used for the real-time system. The calibration model is designed in simulink and the code is generated with real-time workshop. The motor winds the tendon up to the given force ten times. As an example three curves of the force to sensor data are shown in Fig. 9. With rising

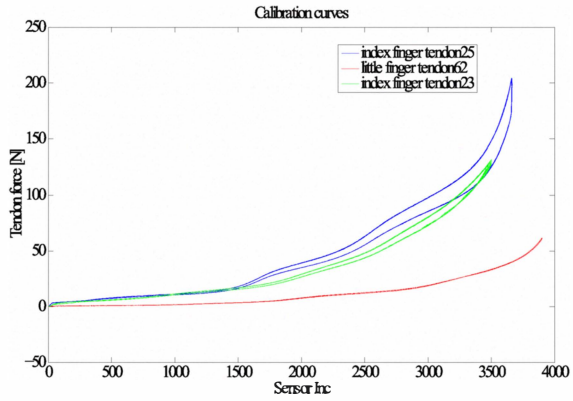

Fig. 9. Force to Sensor Calibration curves of three sensors

force the hysteresis is growing. One reason is the increasing ratio between tendon force and spring force, which causes a higher bearing friction. The nonlinearity of the angle sensor is visible in the calibration curve of index finger tendon 25. For the position measurement of the link the deflection to sensor angle curve is calibrated with the attached hand. Due to the correct tendon length, the complete elastic elongation of the tendon is thus calibrated.

IV. Experiments

A. Validation

To compare the model with the measured data, two different approaches can be used. In Fig. 10 the force to deflection curve is shown. In which the creep of each drive is subtracted. At higher forces the creep during one

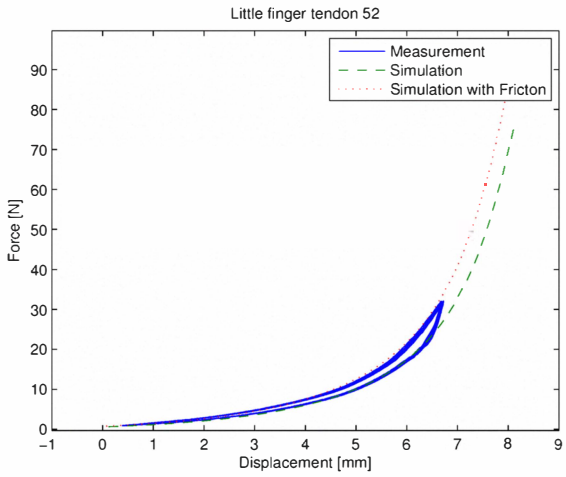

Fig. 10. Comparison of simulation and measurement of force to deflection curve. The major part of the hysteresis comes from the visco elastic effect of the dyneema tendon

preloadphase is to large, to get a good result. The second approach compares the force to angle curve (Fig. 11). A

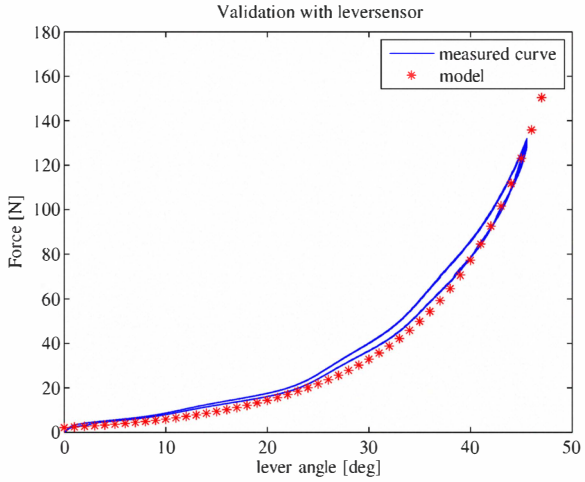

Fig. 11. Validation of force to sensor angle

better validation method is reached, if the sensor is linear.

B. Impedance control of the finger

One function of the FAS is designed to measure the tendon force to control the impedance of the fingers. Fig. 12 shows the control design. The inner force controller keep the tendons always on a minimum pretension to prevent slack. For the test (see Fig.: 13) a extra output sensor was mounted to measure the real angle. The measured compliant (h_{Lever}) in the lever helps to compensate a part of the joint friction in the finger. If the finger is controlled without the feedback of h_{Lever} the position error is three times higher and the controller stiffness must be much higher.

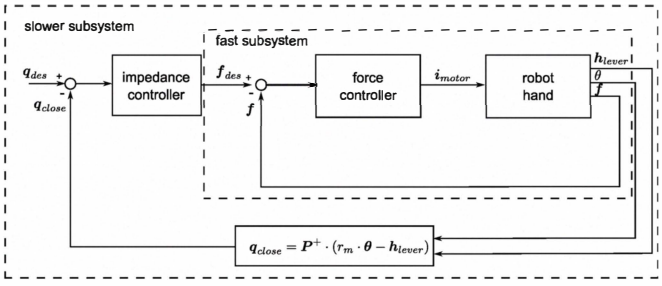

Fig. 12. Design of the joint impedance controller

C. Robustness and dynamic enhancement

In [1] the robustness against hard contacts was demonstrated. A hammer hits the finger at the DIP joint of the index finger. The complete forearm was not mounted on the robot but on a table. Fig. 14 shows the resulting torques and joint velocities. All motors are controlled using a simple position controller. In comparsion to the finger testbed (see [16]) the spring energy is better used because the FAS are fitting to the corresponding finger . Also the inertia of the mechanism is reduced more than twice. Thereby the maximum velocity of the finger can be doubled while the finger is flipping [6].

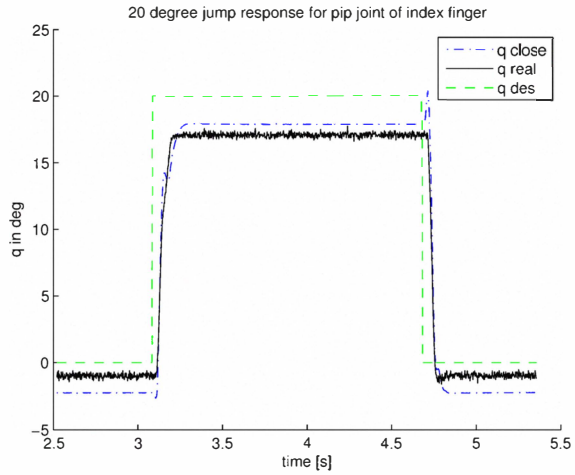

Fig. 13. Step response of the controller after 20 Steps

The inertia of the fingers is too low to load the spring by fast motor moments. Similar to the humans the finger must be fixed by a second finger and then released fast to flip the finger. The maximum measured link speed was over 3500 degree/s after releasing the finger (Fig. 15).

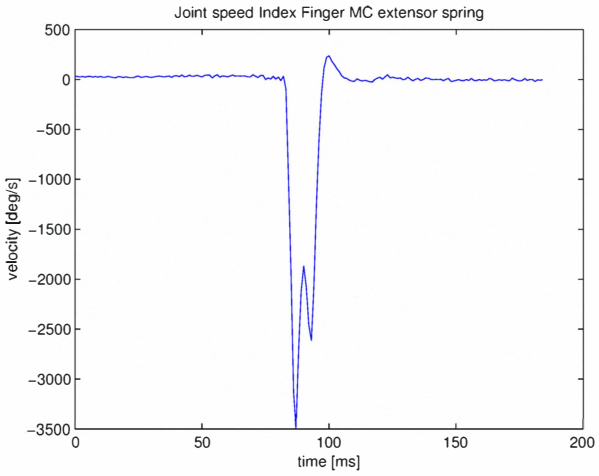

Fig. 15. Index metacarpal joint velocity while flipping the finger

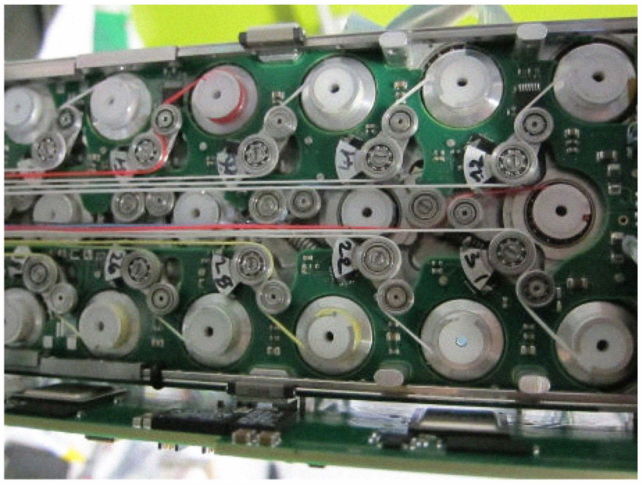

Fig. 16. Upper half of the forearm with 19 FAS

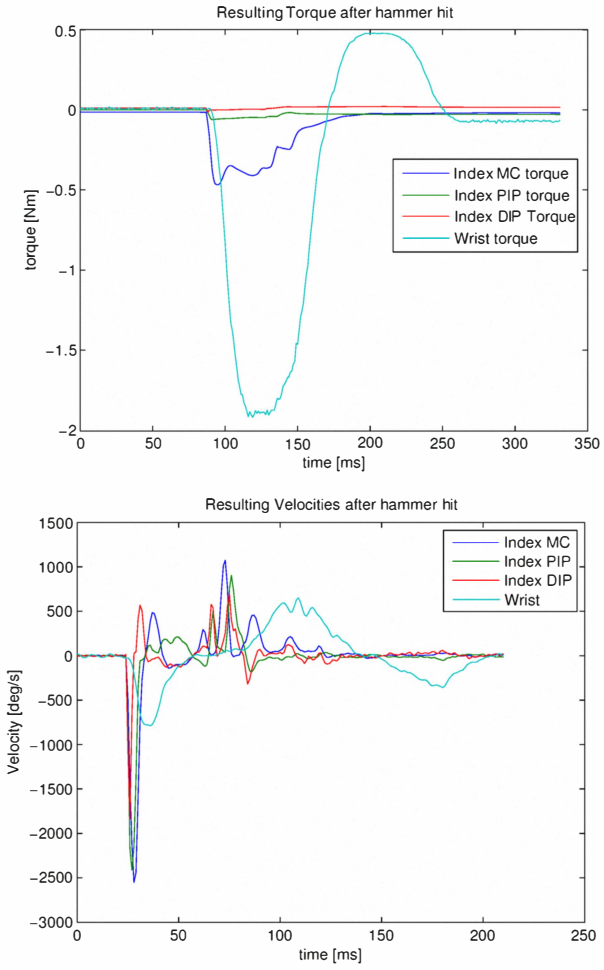

Fig. 14. Resulting torque and velocities after a hammer hits the dip joint of the index finger. The amplitudes after the first one are results of the coupling between wrist and fingers

V. Conclusions

The spring mechanism for an antagonistic tendon driven hand introduced in this paper, called FAS, showed its design flexibility to adapt on 38 various force and deflection requirements in the forearm of the DLR hand-arm system. The developed sensor fulfils the design goals to be very compact and precise. Furthermore the tendon tests demonstrate that dyneema tendons have the characteristics needed for a tendon driven hand, because of the better material properties as other tendons materials. Due to the material properties of dyneema the actuator system has to be able to compensate the creep of the tendons. The shown antagonistic mechanism with its sensor complies with this demand and enabled a high integrated design combined with the drives for hyper actuated robot hand.

VI. Future works

The next step is to enhance the linearity of the sensor with improved magnets. Furthermore the internal sensor calibration options should be used. With in the angle error is calculated by the motor encoder and lever sensor while a pretension. The sensor calibration principle was used in the motor modules and can reduce the angle error about 75 percent. Further a model of the visco elastic effect of the dyneema tendon will be designed to improve the control.

VII. Acknowledgments

This work has been partially funded by the European Commissions Sixth Framework Program as part of the project PHRIENDS under grant no. 045359 and the project VIACTORS under grant no. 231554.

References

[1] M. Grebenstein, A. Albu-Schaffer, T. Bahls, M. Chalon, O. Eiberger, W. Friedl, R. Gruber, U. Hagn, R. Haslinger, H. Hoppner, S. Jorg, M. Nickl, A. Nothhelfer, F. Petit, J. Reill, N. Seitz, T. Wimbock, S. Wolf, T. Wusthoff, and G. Hirzinger, "The dlr hand arm system," in *in Proceedings of the 2011 IEEE International Conference on Robotics and Automation*, 2011.

[2] S. Haddadin, A. Albu-Schaffer, O. Eiberger, and G. Hirzinger, "New insights concerning intrinsic joint elasticity for safety," in *Proc. IEEE/RSJ Int Intelligent Robots and Systems (IROS) Conf*, 2010, pp. 2181–2187.

[3] A. Bicchi, S. L. Rizzini, and G. Tonietti, "Compliant design for intrinsic safety: general issues and preliminary design," in *Proc. IEEE/RSJ Int Intelligent Robots and Systems Conf*, vol. 4, 2001, pp. 1864–1869.

[4] G. Tonietti, R. Schiavi, and A. Bicchi, "Design and control of a variable stiffness actuator for safe and fast physical human/robot interaction," in *Proc. IEEE Int. Conf. Robotics and Automation ICRA 2005*, 2005, pp. 526–531.

[5] S. R. C. Limited, "Shadow dextrous hand product specification," Shadow Robot Company Limited, Tech. Rep., February 2004.

[6] M. Grebenstein and P. van der Smagt, "Antagonism for a highly anthropomorphic handarmsystem," *Advanced Robotics*, vol. 22, pp. 39–55, 2008.

[7] F. Petit, M. Chalon, W. Friedl, M. Grebenstein, A. A. Schaeffer, and G. Hirzinger, "Bidirectional antagonistic variable stiffness actuation: Analysis, design & implementation," in *Proc. IEEE Int Robotics and Automation (ICRA) Conf*, 2010, pp. 4189–4196.

[8] S. A. Migliore, E. A. Brown, and S. P. DeWeerth, "Biologically inspired joint stiffness control," in *Proc. IEEE Int. Conf. Robotics and Automation ICRA 2005*, 2005, pp. 4508–4513.

[9] J. Kobayashi, K. Okumura, Y. Watanabe, and N. Suzuki, "Development of variable stiffness joint drive module and experimental results of joint angle control," in *Proc. of The Fifteenth International Symposium on Artificial Life and Robotics*, 2010, pp. 946–949.

[10] A. Jafari, N. G. Tsagarakis, B. Vanderborght, and D. G. Caldwell, "A novel actuator with adjustable stiffness (awas)," in *Proc. IEEE/RSJ Int Intelligent Robots and Systems (IROS) Conf*, 2010, pp. 4201–4206.

[11] O. Eiberger, S. Haddadin, M. Weis, A. Albu-Schaeffer, and G. Hirzinger, "On joint design with intrinsic variable compliance: derivation of the dlr qa-joint," in *Proc. IEEE Int Robotics and Automation (ICRA) Conf*, 2010, pp. 1687–1694.

[12] R. Schiavi, G. Grioli, S. Sen, and A. Bicchi, "Vsa-ii: a novel prototype of variable stiffness actuator for safe and performing robots interacting with humans," in *Proc. IEEE Int. Conf. Robotics and Automation ICRA 2008*, 2008, pp. 2171–2176.

[13] K. Koganezawa, T. Nakazawa, and T. Inaba, "Antagonistic control of multi-dof joint by using the actuator with non-linear elasticity," in *Proc. IEEE Int. Conf. Robotics and Automation ICRA 2006*, 2006, pp. 2201–2207.

[14] R.-J. Wang and H.-P. Huang, "An active-passive variable stiffness elastic actuator for safety robot systems," in *Proc. IEEE/RSJ Int Intelligent Robots and Systems (IROS) Conf*, 2010, pp. 3664–3669.

[15] S. Wolf, O. Eiberger, and G. Hirzinger, "The DLR FSJ: energy based design of a variable stiffness joint," in *Proc. IEEE Int. Conf. Robotics and Automation ICRA 2011*, 2011.

[16] M. Grebenstein, M. Chalon, G. Hirzinger, and R. Siegwart, "Antagonistically driven finger design for the anthropomorphic dlr hand arm system," in *Proc. 10th IEEE-RAS Int Humanoid Robots (Humanoids) Conf*, 2010, pp. 609–616.